HHS Public Access

Author manuscript

ACS Chem Biol. Author manuscript; available in PMC 2018 January 20.

Published in final edited form as:

ACS Chem Biol. 2017 January 20; 12(1): 200–205. doi:10.1021/acschembio.6b00586.

Live Cell Imaging of Endogenous mRNA using RNA-Based Fluorescence "Turn-On" Probe

Wei Qiang Ong[a], **Y. Rose Citron**[b], **Sayaka Sekine**[a], and **Bo Huang**[*,a]

[a]Department of Pharmaceutical Chemistry, University of California, San Francisco, San Francisco, CA 94143, U.S.A

[b]Graduate Program of Biophysics, University of California, San Francisco, San Francisco, CA 94143, U.S.A

Abstract

Messenger RNA (mRNA) plays a critical role in cellular growth and development. However, there have been limited methods available to visualize endogenous mRNA in living cells with ease. We have designed RNA-based fluorescence "turn-on" probes that target mRNA by fusing an unstable form of Spinach with target-complementary sequences. These probes have been demonstrated to be selective, stable and capable of targeting various mRNAs for live *E. coli* imaging.

The role of messenger RNA (mRNA) as a template for direct protein synthesis obtained from a DNA blue print is well documented in the central dogma. Following the temporal dynamics and spatial localization of mRNA is thus important to understand the regulation of gene expression. mRNA was found to localize asymmetrically within cells for different mRNA processes.[1–3] Bacterial cells, which had long been believed to have freely diffusing mRNA due to its lack of organization, have also been shown to have spatial organization of mRNAs.[4, 5] These localized mRNA, found in both prokaryotes and eukaryotes cells, provides temporal and spatial control of protein expressions which are critical for developmental physiology and cell activity. Hence, it has become increasingly important to visualize endogenous mRNA, and other forms of RNA, in living cells in order to understand the mechanism related to the functions and dynamics of various RNAs and address biological relevant questions so as to be able to provide solutions for diagnostic and therapeutic purposes.

There have been considerable efforts in developing probes and methods for detecting RNA molecules in living cells including emerging technologies such as hybridization chain reactions[6, 7] and templated chemical reactions.[8, 9] Several methods use either organic fluorophore or fluorescence protein (FP) as reporters.[10–14] Targeting with organic probes is

[*]**Corresponding Author:** bo.huang@ucsf.edu.

Supporting Information

Materials, experimental details, sequences of probes used in this study and supplementary figure. This material is available free of charge via the Internet at http://pubs.acs.org.

Notes

The authors declare no competing financial interests.

achieved through single-stranded oligonucleotides (ODNs),[4, 15, 16] locked nucleic acids (LNA)[4] or molecular beacon[17, 18] probes that hybridize to complementary target RNA strand. The fluorescence signal can be observed either directly or through fluorescence resonance energy transfer (FRET). On the other hand, FPs are usually fused to RNA binding proteins, such as bacterial phage coat proteins MS2[19–23], PP7[23, 24], PUMILIO1[25], or dCas9 in the CRISPR system.[26] These proteins will bind to their targeted RNA interacting sequences. An advantage of using FPs over organic fluorophores is that they can be introduced into live cells efficiently with minimal perturbation or probe degradation.[10, 13] However, a limitation of these ODN or FP probes in imaging is the high background from unbound probe.

A more recent method uses an RNA aptamer that binds to pro-fluorescent chromophores and increase their quantum yield.[27–30] These RNA aptamers are usually inserted at the 3′ end of the target RNA. Fluorescence will be observed only upon complexation of the fluorophore to the RNA aptamer, hence reducing the background from the unbound fluorophores in the cytoplasm during live cell imaging.[31–33] Nevertheless, adding the RNA aptamer sequences to the target RNA may affect its expression level and functional activities.[14]

In order to image endogenous mRNAs without having to individually modify the genomic DNA, here we report a method in live *Escherichia coli* (*E. coli*) cells using a fluorescence "turn-on" probe derived and modified from the RNA- fluorophore complex, Spinach.[27, 28] Spinach is a RNA aptamer that emits green fluorescence upon binding to several pro-fluorescent fluorophores that resemble the chromophore of GFP.[35] In this study, we used the first generation 3,5-difluoro-4-hydroxybenzylidene imidazolinone (DFHBI) as the fluorophore. It is worth noting that newer generations of the fluorophore may give brighter signal or different emission wavelengths.[35] Our design principle behind the "turn-on" probe was to use an unstable form of Spinach such that it will be "off"/non-fluorescent, unable to bind DFHBI, unless it is stabilized in complex with its target RNA (Figure 1). Only upon binding with the target RNA is the configuration of Spinach stabilized, allowing DFHBI to bind at its correct position. In this way, there will be no background fluorescence signal from unbound aptamer or fluorophore. Specific labelling of target mRNA can be achieved and observed directly upon DFHBI addition.

In order to create a destabilized form of Spinach, we carried out a rational design approach. Earlier work on the crystal structure of Spinach revealed a double helix structure containing a core G-quadruplex motif, which is responsible for the binding of ligand DFHBI. The core G-quadruplex is sandwiched between two stems (i.e. stem-*a* and *b*). It has been shown that most of the stem-*a* of Spinach is not required to produce fluorescence signal.[34, 36] A truncated version of Spinach containing the core G-quadruplex motif and with five based pairs in stem-*a* (P1-*a5*-*b5*) (Figure 2A) had been shown to retain the same level of fluorescence as Spinach-WT.[34] We note that this truncated sequence had a shorter stem-*b* than Spinach-WT. Using this truncated sequence as the starting point, we tried to determine the smallest functional unit by constructing four shorter probes, in which stems-*a* and *b* of Spinach aptamer P1-*a5*-*b5* had been replaced with base-pairs of shorter length (Figure 2A). The core G-quadruplex motif in Spinach was retained in all truncated probes. The probes were assessed by transformation into *E. coli* cells and measuring the whole cell fluorescence

(Figure 2B). We found that preserving only three Watson-Crick base pairs in stem-*b* (P1-*a5-b3*) retained almost the same level of fluorescence as that of P1-*a5-b5*. Shorter probes with one (P1-*a5-b1*) or no (P1-*a5-b0*) Watson-Crick base pair in stem-*b* gave negligible fluorescence (< 10% of P1-*a5-b5*'s signal). On top of that, reducing the base-pairs from five to four (P1-*a4-b5*) in stem-*a* also led to the loss of Spinach fluorescence (~6% of P1-*a5-b5*'s signal).

The results were further supported by live imaging, where only DFHBI-treated *E. coli* expressing the P1-*a5-b5* and P1-*a5-b3* probes emitted strong green fluorescence, whereas the fluorescence signal from other truncated probes were close to the autofluorescence level (Figure 2D). The excitation and emission spectra of P1-*a5-b5*-DFHBI and P1-*a5-b3*-DFHBI (Figure 2C) obtained were identical, which suggests that the shorter P1-*a5-b3* was able to fold into the same configuration as Spinach, allowing the DFHBI to bind to the top of the G-quadruplex motif.

We also note that in the earlier truncation work where the fluorescence was determined *in vitro*,[34] a construct with three base pairs in stem-*a* (P2) emitted fluorescence which is about 70% of Spinach-WT. In contrast, our live *E. coli* measurement detected almost no fluorescence despite having four thermodynamically stable G-C base pairing in stem-*a*. These results indicated that P1-*a5-b3* (52 bases long) is the smallest Spinach aptamer that is functional in *E. coli*.

Because the mini-Spinach aptamer with only four base pairs in stem-*a* (P1-*a4-b5*) does not fluoresce, whereas the one with five base pairs (P1-*a5-b5*) is fluorescent, P1-*a4-b5* is an ideal candidate for hybridization probes that could be turn-on upon binding to target mRNAs. To design such a probe, we attached the complementary sequences to a short segment of a mRNA of interest to the 5′ and 3′ ends of the probe. The probe itself would be non-fluorescence. Upon hybridization of the probe to the target mRNA, the mRNA target will stabilize the probe, resulting in the probe folding into the correct conformation that allows the DFHBI ligand to bind and emit fluorescence (Figure 1). Two versions of the probe were created, one containing three base pairs (i.e. P3-*a4-b3*) and another one containing five base pairs (i.e. P3-*a4-b5*) respectively in stem-*b* (Figure 2A). These probes are referred to as P3-*3* and P3-*5* respectively in the rest of the article. We tested our design by selecting a 22 base region of a target mRNA, fusing its complementary sequences to P3 (11 bases on each end), expressing the probe in *E. coli*, and imaging the cells live after the addition of DFHBI.

We first tested a probe targeting the region of nucleotide 35 to 56 of mRNA *mreB* ($mreB_{35–56}$), an abundant mRNA of an actin-like protein in *E. coli*. As the control, two additional probes were designed that contained one and two mismatches, respectively, on each side of the complementary sequences (Figure 3A). While the matched probe produced strong fluorescence signal from live, DFHBI-treated *E. coli*, negligible fluorescence signals were obtained from the two mismatched probes under the same condition (Figure 3A, II–III), suggesting that the probe was highly specific towards it target. A single or two bases mutation would cause the probe to either bind to its target weakly or fold incorrectly, resulting in an absence of fluorescence signal. Reducing the number of complementary

bases from 11 to 9 on each side also resulted in the loss of fluorescence signal (Figure 3A, IV) suggesting that a minimum of 11 bases on each side of the stem was required for proper stabilization of the Spinach configuration. If we treat the average signal of II, III and IV as the basal fluorescence from the probe itself, mreB probe I has a fluorescence turn-on ratio of ~ 10 (autofluorescence from wild-type cells subtracted).

We further examined five more probes targeting a short region of mRNAs for *adk, dnaJ, dnaK, mreB* and *rpoH* in *E. coli*. All of them showed strong fluorescence in DFHBI-treated cells, confirming the generality of our turn-on probe design (Figure 3B). Our second mreB probe targeting nucleotide 934 to 955 actually showed more than twice as high signal as the first one, suggesting that the sensitivity of our probes is sequence-dependent. From the wild-type cell background, the average signal from six probes (Figure 3C), and RNA sequencing data for this E. coli strain, we estimate the detection limit to be approximately 65 reads per kilobase per million mapped reads (RPKM). RNA sequencing data show that under wild-type conditions ~1350 *E. coli* genes have expression levels higher than this limit and thus can theoretically be detected by our method.

In order to check whether probe binding affects the stability of the target mRNA, we used RT qPCR to examine the level of mreB mRNA in E. coli expressing either probes targeting or not targeting mreB sequence (Supporting Information Figure S1). We found no significant difference between the two groups ($p = 0.56$, unpaired t-test).

One potential concern in the probe design is the possible self-complementation if the first base on the two sides of stem-*a* could base-pair to form either Watson-Crick base-pair, wobble base pair G–U or non-canonical base pairs such as U–U and A–A. This situation might lead to false positive results from a 5 base-pairs pairing in stem-*a* (Figure 4A). To test this case, we chose two different regions of *mreB* mRNA such that the first bases of the complementary sequence that was attached to stem-*a* would resulted in a strong G-C base pair.

For the negative controls, the exact same sequences of the targets were used in the probe. Hence, the resultant probes would not be able to bind to their target, but they could potentially still form a stem-*a* with 5 base-pairs due to the G-C bond, resulting in fluorescence. Interestingly, when expressing these probes in *E. coli*, only the probes with target-complementary sequences gave out fluorescence signal after DFHBI-treatment (Figure 4B). In contrast, the two probes with target-identical sequences remained dark, potentially because the non-complemented region of the probe arms destabilize stem-*a* folding. This result further validated the fact that the probe is highly specific towards its target.

In summary, we have designed, synthesized and characterized a RNA-based fluorescence “turn-on” probe for live cell mRNA imaging by fusing an unstable form of Spinach with the target’s complementary sequences. These fluorescent “turn-on” probes had been demonstrated to be selective and robust for various mRNA targets. Our method has the advantages of being able to target endogenous mRNAs, live cell compatibility and minimal background from the free unbound probe. However, the current version of the probe still has

a few limitations. It is much dimmer than organic dyes and thus making it difficult to visualize mRNA with low copies number or that localizes at the poles of the *E. coli* cells. Ongoing work will focus on improving the brightness of these first generation probes and apply them in mammalian cell systems.

Supplementary Material

Refer to Web version on PubMed Central for supplementary material.

Acknowledgments

We thank M.C. Hammond, P. Yin and A.A. Green for insightful discussions. We thank Y. Zhang and C. Gross for providing the *E. coli* RNA-seq data. This work was supported by NIH Director's New Innovator Award (DP2OD008479) and the NIH Extracellular RNA Communication Consortium (U19CA179512). Y.R. Citron acknowledges support by the NSF Graduate Research Fellowship. S. Sekine thankfully acknowledges support by Japan Society for the Promotion of Science Postdoctoral Fellowship for Research Abroad.

References

1. Lécuyer E, Yoshida H, Parthasarathy N, Alm C, Babak T, Cerovina T, Hughes TR, Tomancak P, Krause HM. Global Analysis of mRNA Localization Reveals a Prominent Role in Organizing Cellular Architecture and Function. Cell. 2007; 131:174–187. [PubMed: 17923096]
2. Martin KC, Ephrussi A. mRNA Localization: Gene Expression in the Spatial Dimension. Cell. 2009; 136:719–730. [PubMed: 19239891]
3. Weatheritt RJ, Gibson TJ, Babu MM. Asymmetric mRNA localization contributes to fidelity and sensitivity of spatially localized systems. Nat Struct Mol Biol. 2014; 21:833–839. [PubMed: 25150862]
4. Montero Llopis P, Jackson AF, Sliusarenko O, Surovtsev I, Heinritz J, Emonet T, Jacobs-Wagner C. Spatial organization of the flow of genetic information in bacteria. Nature. 2010; 466:77–81. [PubMed: 20562858]
5. Keiler KC. RNA localization in bacteria. Curr Opin Microbiol. 2011; 14:155–159. [PubMed: 21354362]
6. Choi HMT, Chang JY, Trinh LA, Padilla JE, Fraser SE, Pierce NA. Programmable in situ amplification for multiplexed imaging of mRNA expression. Nat Biotech. 2010; 28:1208–1212.
7. Choi HMT, Beck VA, Pierce NA. Next-Generation in Situ Hybridization Chain Reaction: Higher Gain, Lower Cost, Greater Durability. ACS Nano. 2014; 8:4284–4294. [PubMed: 24712299]
8. Abe H, Kool ET. Flow cytometric detection of specific RNAs in native human cells with quenched autoligating FRET probes. Proc Natl Acad Sci USA. 2006; 103:263–268. [PubMed: 16384914]
9. Holtzer L, Oleinich I, Anzola M, Lindberg E, Sadhu KK, Gonzalez-Gaitan M, Winssinger N. Nucleic Acid Templated Chemical Reaction in a Live Vertebrate. ACS Cent Sci. 2016; 2:394–400. [PubMed: 27413783]
10. Tyagi S. Imaging intracellular RNA distribution and dynamics in living cells. Nat Methods. 2009; 6:331–338. [PubMed: 19404252]
11. Bao G, Rhee WJ, Tsourkas A. Fluorescent Probes for Live-Cell RNA Detection. Annu Rev Biomed Eng. 2009; 11:25–47. [PubMed: 19400712]
12. Weil TT, Parton RM, Davis I. Making the message clear: visualizing mRNA localization. Trends Cell Biol. 2010; 20:380–390. [PubMed: 20444605]
13. Park, HY., Buxbaum, AR., Singer, RH. Chapter 18 - Single mRNA Tracking in Live Cells. In: Nils, GW., editor. Methods Enzymol. Academic Press; 2010. p. 387-406.
14. Broude NE. Analysis of RNA localization and metabolism in single live bacterial cells: achievements and challenges. Mol Microbiol. 2011; 80:1137–1147. [PubMed: 21453445]
15. Lu J, Tsourkas A. Imaging individual microRNAs in single mammalian cells in situ. Nucleic Acids Res. 2009; 37:e100. [PubMed: 19515934]

16. Lubeck E, Cai L. Single-cell systems biology by super-resolution imaging and combinatorial labeling. Nat Methods. 2012; 9:743–748. [PubMed: 22660740]
17. Bratu DP, Cha BJ, Mhlanga MM, Kramer FR, Tyagi S. Visualizing the distribution and transport of mRNAs in living cells. Proc Natl Acad Sci USA. 2003; 100:13308–13313. [PubMed: 14583593]
18. Murayama K, Kamiya Y, Kashida H, Asanuma H. Ultrasensitive Molecular Beacon Designed with Totally Serinol Nucleic Acid (SNA) for Monitoring mRNA in Cells. ChemBioChem. 2015; 16:1298–1301. [PubMed: 25851922]
19. Fusco D, Accornero N, Lavoie B, Shenoy SM, Blanchard JM, Singer RH, Bertrand E. Single mRNA Molecules Demonstrate Probabilistic Movement in Living Mammalian Cells. Curr Biol. 2003; 13:161–167. [PubMed: 12546792]
20. Nevo-Dinur K, Nussbaum-Shochat A, Ben-Yehuda S, Amster-Choder O. Translation-Independent Localization of mRNA in E. coli. Science. 2011; 331:1081–1084. [PubMed: 21350180]
21. Shav-Tal Y, Darzacq X, Shenoy SM, Fusco D, Janicki SM, Spector DL, Singer RH. Dynamics of Single mRNPs in Nuclei of Living Cells. Science. 2004; 304:1797–1800. [PubMed: 15205532]
22. Brodsky AS, Silver PA. Identifying proteins that affect mRNA localization in living cells. Methods. 2002; 26:151–155. [PubMed: 12054891]
23. Wu B, Chen J, Singer RH. Background free imaging of single mRNAs in live cells using split fluorescent proteins. Sci Rep. 2014; 4:3615. [PubMed: 24402470]
24. Lim F, Peabody DS. RNA recognition site of PP7 coat protein. Nucleic Acids Res. 2002; 30:4138–4144. [PubMed: 12364592]
25. Ozawa T, Natori Y, Sato M, Umezawa Y. Imaging dynamics of endogenous mitochondrial RNA in single living cells. Nat Methods. 2007; 4:413–419. [PubMed: 17401370]
26. Nelles DA, Fang MY, O'Connell MR, Xu JL, Markmiller SJ, Doudna JA, Yeo GW. Programmable RNA Tracking in Live Cells with CRISPR/Cas9. Cell. 2016; 165:488–496. [PubMed: 26997482]
27. Paige JS, Wu KY, Jaffrey SR. RNA Mimics of Green Fluorescent Protein. Science. 2011; 333:642–646. [PubMed: 21798953]
28. Strack RL, Disney MD, Jaffrey SR. A superfolding Spinach2 reveals the dynamic nature of trinucleotide repeat-containing RNA. Nat Methods. 2013; 10:1219–1224. [PubMed: 24162923]
29. Filonov GS, Moon JD, Svensen N, Jaffrey SR. Broccoli: Rapid Selection of an RNA Mimic of Green Fluorescent Protein by Fluorescence-Based Selection and Directed Evolution. J Am Chem Soc. 2014; 136:16299–16308. [PubMed: 25337688]
30. You M, Jaffrey SR. Structure and Mechanism of RNA Mimics of Green Fluorescent Protein. Annu Rev Biophys. 2015; 44:187–206. [PubMed: 26098513]
31. Höfer K, Langejürgen LV, Jäschke A. Universal Aptamer-Based Real-Time Monitoring of Enzymatic RNA Synthesis. J Am Chem Soc. 2013; 135:13692–13694. [PubMed: 23991672]
32. Pothoulakis G, Ceroni F, Reeve B, Ellis T. The Spinach RNA Aptamer as a Characterization Tool for Synthetic Biology. ACS Synth Biol. 2014; 3:182–187. [PubMed: 23991760]
33. Strack, RL., Jaffrey, SR. Chapter Seven - Live-Cell Imaging of Mammalian RNAs with Spinach2. In: Donald, HB-A., editor. Methods Enzymol. Academic Press; 2015. p. 129-146.
34. Huang H, Suslov NB, Li NS, Shelke SA, Evans ME, Koldobskaya Y, Rice PA, Piccirilli JA. A G-quadruplex–containing RNA activates fluorescence in a GFP-like fluorophore. Nat Chem Biol. 2014; 10:686–691. [PubMed: 24952597]
35. Song W, Strack RL, Svensen N, Jaffrey SR. Plug-and-Play Fluorophores Extend the Spectral Properties of Spinach. J Am Chem Soc. 2014; 136:1198–1201. [PubMed: 24393009]
36. Warner KD, Chen MC, Song W, Strack RL, Thorn A, Jaffrey SR, Ferré-D'Amaré AR. Structural basis for activity of highly efficient RNA mimics of green fluorescent protein. Nat Struct Mol Biol. 2014; 21:658–663. [PubMed: 25026079]

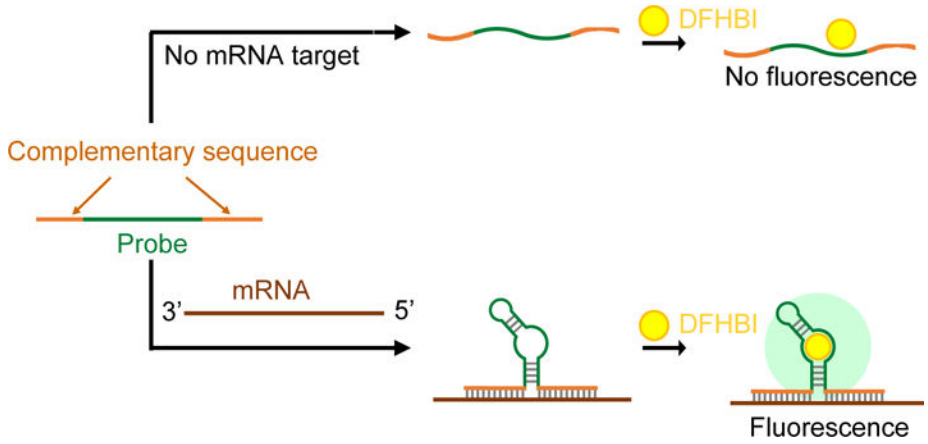

Figure 1.

Design scheme for using an unstable form of Spinach to detect endogenous mRNA. Binding of the complementary sequences (orange) to the target mRNA (brown) enables the mini-Spinach probe (green) to be able to bind the ligand DFHBI and produce green fluorescence.

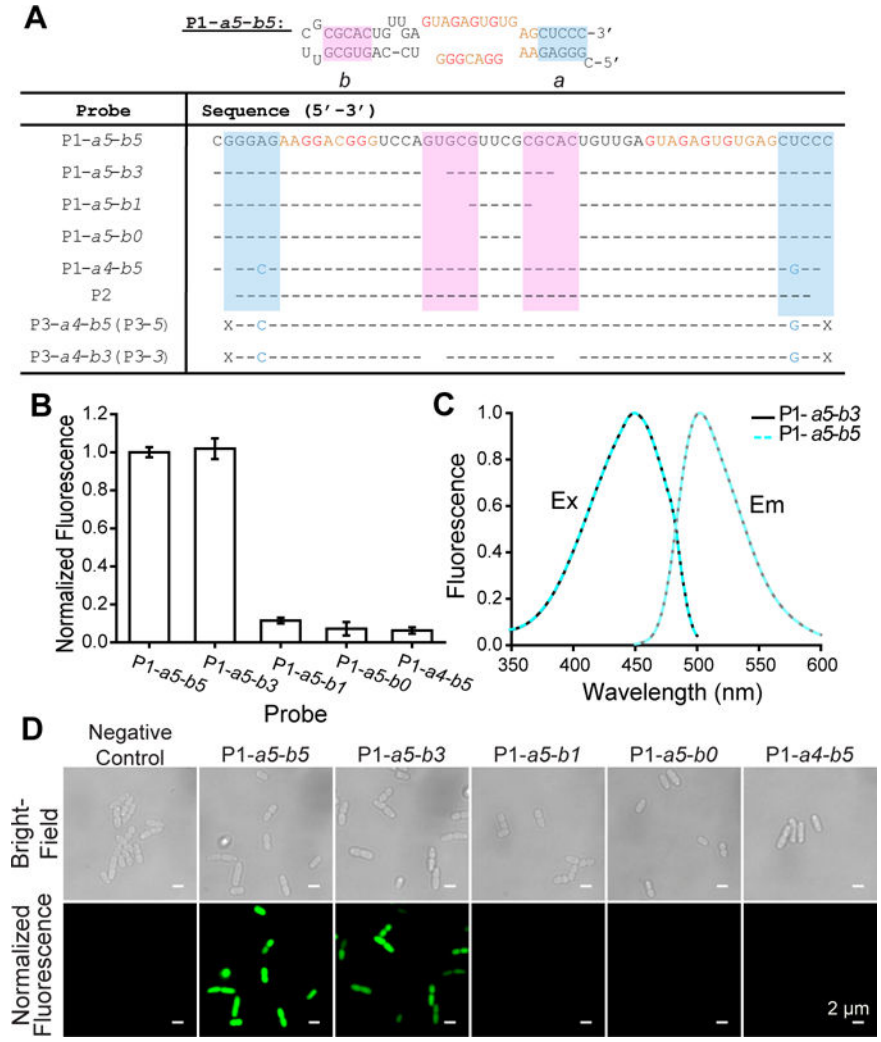

Figure 2.

mini-Spinach probe. A) Sequences of the various mini-Spinach probes used in the study are shown in the table. The secondary structure of mini-Spinach probe P1-*a5-b5* is shown above the table (Ref. 34). The core G-quadruplex motif in the probe where the DFHBI ligand binds to is shown in orange and red, with the participating Gs in red. Stem-*a* (highlighted in blue) and stem-*b* (highlighted in pink) are truncated to produce the other mini-Spinach truncated probes. Base mutations from P1-*a5-b5* are shown at the respective positions in blue. Unaltered bases are indicated by dashes and an absence of dashes at the respective position indicates deletion of bases. The complementary sequences to the target mRNA are indicated by 'X' in probe P3. B) Normalized whole cell fluorescence of DFHBI-treated *E. coli* cells expressing the various mini-Spinach probes. The measurements are normalized to the fluorescence intensity of P1-*a5-b5* after subtracting the background measured in untransformed cells. Data represent mean values ± s.e.m. from three measurements. C) Excitation and emission spectra of P1-*a5-b5*-DFHBI and P1-*a5-b3*-DFHBI. Spectra were measured using 20 μM RNA and 2 μM DFHBI. D) Bright-field and normalized fluorescence images of live untransformed cells (negative control) and live DFHBI-treated *E. coli* expressing the various mini-Spinach probes. Scale bar = 2 μm.

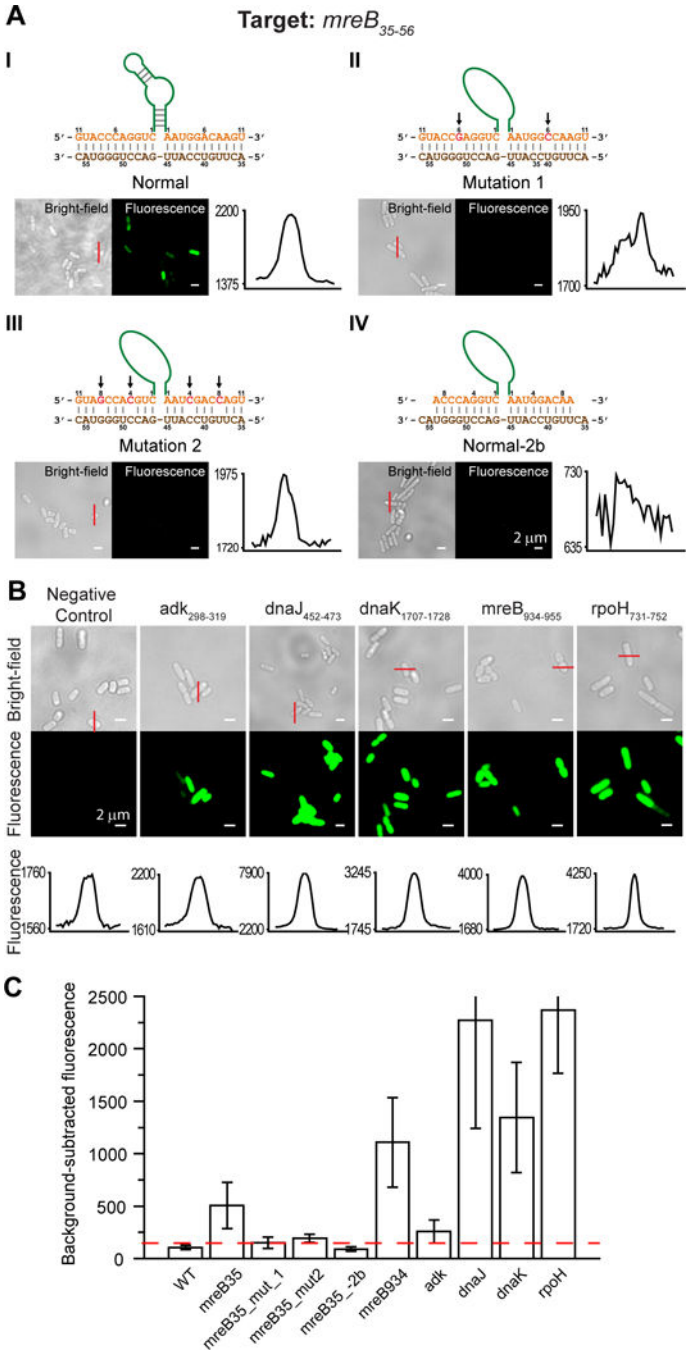

Figure 3.

mRNA imaging using mini-Spinach probe. A) P3-*5* probes targeting *mreB*$_{35–56}$ with having I) zero, II) one (at position 6), III) two (at positions 4 and 8) mutations and IV) two fewer bases on each side in the complementary sequence (shown in orange). The sequence of the target *mreB*$_{35–56}$ is shown in brown. The mutations are shown in red and its positions are indicated by the arrow. Bright-field and fluorescence images of live DFHBI-treated *E. coli* expressing these 4 probes are shown, with the fluorescence images adjusted to the same contrast. A profile across one cell is plotted for each image (y axes in camera counts). B)

Bright-field and fluorescence images of live DFHBI-treated *E. coli* expressing P3–3 probes that target various mRNAs targets (italic) at 37 °C. The fluorescence images are adjusted to the same contrast and cross sections are plotted in the same way as in (A). The number range in subscript after the mRNA target represents the targeted nucleotide positions on the mRNA. Scale bar = 2 μm. C) Background-corrected fluorescence signal level for all samples, showing mean ± standard deviation from 30 cells in each case. The red dashed line marks the detection limit defined wild-type baseline + 2 × standard deviation.

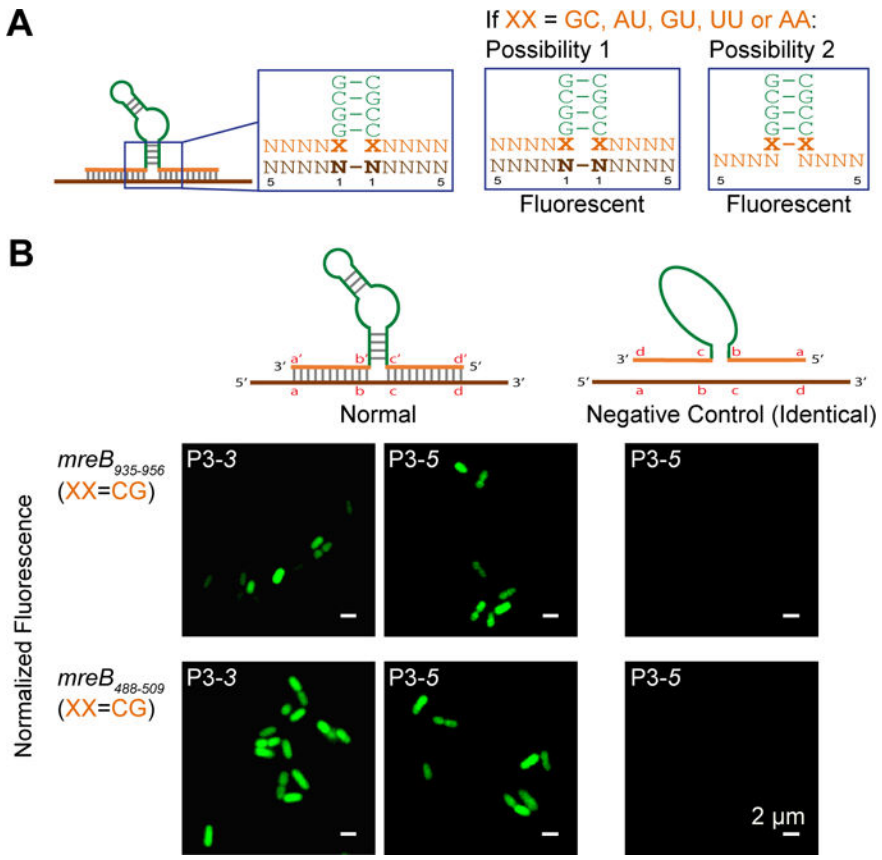

Figure 4.

Test for potential alternative binding mode. A) The two possible binding modes when the first complementary base (X) on both side of stem-*a* of the mini-Spinach probe P3 is capable of base-pairing with each other. B) Normalized fluorescence images of live DFHBI-treated *E. coli* expressing P3 probes targeting $mreB_{935–956}$ and $mreB_{488–509}$. In the negative controls, the sequence of the target was attached to the probe instead of its complementary sequences. In all case, XX = C–G. Since negligible fluorescence was observed in the negative control cases, it showed that the chance of Possibility 2 (in (A)) occurring in the cell was very low and the target was required for the probe to be stable and to fold into the correct configuration. Scale bar = 2μm.